

## Article

# Experimental Study of LiCl/LiBr-Zeolite Composite Adsorbent for Thermochemical Heat Storage

Depeng Chen <sup>1</sup>, Xin Chen <sup>1</sup>, Zhiwei Ma <sup>2</sup>, Yaodong Wang <sup>2</sup>, Anthony Paul Roskilly <sup>2</sup> and Jian Zhou <sup>2,\*</sup><sup>1</sup> School of Architecture and Engineering, Anhui University of Technology, Maanshan 243000, China<sup>2</sup> Department of Engineering, Durham University, Durham DH1 3LE, UK

\* Correspondence: jian.zhou@durham.ac.uk; Tel.: +44-(0)-7533095659

**Abstract:** Adsorption-based thermochemical heat storage is a promising long-term energy storage technology that can be used for seasonal space heating, which has received significant amount of efforts on the research and development. In this paper, the heat storage capacity of composite adsorbents made by LiCl + LiBr salt and 3A zeolite was investigated. The basic characteristics of composite material groups were experimentally tested, and it was found that the adsorption composite with 15 wt% salt solution had excellent adsorption rate and adsorption capacity, which was considered as the optimal composite material. Furthermore, the heat storage density of the composite material could be as high as 585.3 J/g, which was 30.9% higher than that of pure zeolite. Using 3 kg of the composite material, the adsorption heat storage experiment was carried out using a lab-scale reactor. The effects of air velocity and relative humidity on the adsorption performance were investigated. It was found that a flow rate of 15 m<sup>3</sup>/h and a relative humidity of 70% led to the most released adsorption heat from the composite material, and 74.3% of energy discharge efficiency. Furthermore, an adsorption heat storage system and a residential model were built in the TRNSYS software to evaluate the building heating effect of such heat storage system. It is found that the ambient temperature will affect the heating effect of the adsorption heat storage system. The coefficient of performance (COP) of this model is as high as 6.67. Compared with the gas boiler heating system, the adsorption heat storage energy can replace part of the gas consumption to achieve energy savings.

**Keywords:** thermochemical heat storage; hygroscopic salt; zeolite; water vapour sorption; energy discharge efficiency; TRNSYS; building model



**Citation:** Chen, D.; Chen, X.; Ma, Z.; Wang, Y.; Roskilly, A.P.; Zhou, J. Experimental Study of LiCl/LiBr-Zeolite Composite Adsorbent for Thermochemical Heat Storage. *Buildings* **2022**, *12*, 2001. <https://doi.org/10.3390/buildings12112001>

Academic Editors: Shi-Jie Cao and Wei Feng

Received: 10 October 2022

Accepted: 11 November 2022

Published: 17 November 2022

**Publisher's Note:** MDPI stays neutral with regard to jurisdictional claims in published maps and institutional affiliations.



**Copyright:** © 2022 by the authors. Licensee MDPI, Basel, Switzerland. This article is an open access article distributed under the terms and conditions of the Creative Commons Attribution (CC BY) license (<https://creativecommons.org/licenses/by/4.0/>).

## 1. Introduction

Energy consumption in buildings has steadily increased in recent years. Fossil fuels are increasingly becoming unviable as an energy source due to the rapidly increasing global population and growing demands of urban construction. Instead, a range of ecologically sound renewable energy sources, such as solar, wind, and biomass energy, are increasingly being developed to supply energy demands [1–4]. This transition to renewable energy is important to slow climate change and reduce the usage of fossil fuel resources. However, at present, there is a mismatch between user demand and the supply of most renewable energy sources. For example, solar energy is an effective alternative to fossil fuels for heating buildings, which is abundant, however it is intermittent and unstable because the solar radiation varies with weather conditions and time of a day [5]. Most of the solar energy supply is in the summer, heating is most needed in the winter when solar energy is less abundant [6]. Therefore, the reasonable utilization of solar energy requires new technologies to realise short to long term heat storage.

Thermal energy storage (TES) can be used to resolve the timing mismatch between solar energy supply and energy demand [7,8]. There is increasing interest in technically advanced and economical TES systems for applications such as hot water supply and

space heating. Among them, thermochemical heat storage (TCHS) systems have many advantages over other types of TES [9,10]. This method involves storing energy through reversible adsorption processes or chemical reaction, thus, high reaction enthalpies can be used to achieve greater energy storage density, making the system appropriate for large-scale applications. Using this method, the heat loss during the energy storage process is almost zero [11,12]; in addition, due to controllable gas partial pressure, this technology is capable of heating, cooling and thermal energy storage functions, allowing the conversion of heat within a specific temperature range [13]. Such feature provides more flexibility than traditional heat storage systems. Moreover, long-term seasonal storage for buildings can be achieved by using TCHS because the heat is stored as chemical potential, which does not degrade over time [14–17].

Hygroscopic salts have been extensively investigated as one of the most promising materials for TCHS applications. These salts have high water absorption capability and heat storage density [18,19] and have been identified as suitable thermal storage candidates in the temperature range of 20 to 200 °C [20,21]. Typical hygroscopic salts for TCHS are  $\text{CaCl}_2$  and  $\text{MgCl}_2$  [22],  $\text{LiCl}$  [23,24] and  $\text{MgSO}_4$  [25,26]. In [27],  $\text{LiCl}$  composites showed higher adsorption capacity, closely followed, in order, by  $\text{CaCl}_2$  and  $\text{LiBr}$  composites. By mixing other salts,  $\text{LiI}$ ,  $\text{LiNO}_3$ ,  $\text{LiCl}$ , etc., into the  $\text{LiBr}$  solution, mixed materials have been developed aiming to improve solubility, corrosion and stability [28,29], which inspired the development of composite material using mixed salts. Gordeeva et al. [30] found that dual salt composite adsorbents could reduce adsorption hysteresis while having the potential to significantly improve flexibility and operational reliability, and they designed binary  $\text{LiCl}$ - $\text{LiBr}$  systems confined in silica pores as effective materials with predetermined adsorption properties. Entezari et al. [31] discovered that adding a small amount of  $\text{LiBr}$  to  $\text{LiCl}$  can improve the adsorption capacity of the binary salt composites by up to 5.5%, and he used simulations to evaluate the dehumidification performance of the adsorbent.

In practical system applications, deliquescence of hygroscopic salts leads to the leakage of the liquid salty solution and loss of salt, thus reducing the cyclic stability [32]. To improve the usage of hygroscopic salts, researchers have investigated embedding the salts in porous structures, which are used as carriers to immobilize inorganic salts and distribute them uniformly. Furthermore, the porous properties of the carrier increase the surface area of the composite adsorbent—these materials enhance the heat and mass transfer efficiency with increasing surface area [33]. Commonly used porous matrix (CSPM) include silica gel [34,35], zeolite [36,37] and expanded graphite [38]. Zeolites are porous materials with good water absorption capacity and the ability to function at high temperatures, thus forming excellent matrices for composite materials [39]. Thomas et al. [40] developed composite adsorbent by impregnating zeolites with salt solutions and concluded that the impregnation of these salts by zeolite allowed salt deliquescence and water absorption above the deliquescence humidity, without the problem of leakage and loss of salt. With high salt loading ratio and at high air humidity levels, the heat storage density of composite material can be up to 153% of that of pure zeolite. Gareth et al. [6] developed four zeolite composites impregnated with different mass fractions of  $\text{MgSO}_4$ ; their results showed a strong correlation between the microstructure of zeolite and the heat generated by the composite. To avoid deliquescence, the mass concentration of hygroscopic salts in the composites was usually limited to below 35%.

Previous studies on composite adsorbents have focused on characterising small amount of materials [41–43]. These studies have been less further investigated by applying the materials to real practical systems. System design is the key to developing architectural applications for TCHS. In the current study, the deployment of conventional filled beds in energy storage systems suffers from low energy storage density and large volume. Effective ways to solve such problems and reduce potential costs are worth being explored [44]. Addressing this research goal, Calabrese [45] evaluated the performance of foam-based adsorbent materials in open and closed adsorption heat storage applications and pointed out that matrix maintenance of cyclic stability in practical applications is an

important issue to be addressed. Xu et al. [46] developed a numerical model to investigate the thermochemical reaction process in a reactor filled with composite adsorbent and calculated the heat transfer between the composite material and water vapour. Li et al. [47] numerically developed a novel multi-layered sieve reactor focusing on the interaction between the composite material and the air in an open system; in addition, they performed a parametric analysis of the inlet temperature, humidity and airflow rate. Future more, it is expected that the TCHS system will be applied to actual residential heating. A laboratory prototype of a fixed-bed open TCHS reactor developed by Zondag et al. [22] can provide a certain amount of thermal energy for home heating. The system contains 17 dm<sup>3</sup> of adsorbent material, which can generate 150 W of thermal energy and achieve an effective energy storage density of about 0.5 GJ/m<sup>3</sup>. Consider time period and material cost constraints when using energy from TCHS systems for home construction. Researchers can use the TRNSYS program to simulate and analyze transient systems. Safa et al. [48] simulated the heating performance of the heat pump system in the TRNSYS environment and found that the coefficient of performance (COP) under different heat source temperatures was 3.05–3.44 during heating. In TRNSYS-EES, Sakellari et al. [49] analyzed the performance of a heating system based on an exhaust air heat pump using simulation. And several strategies have been proposed to keep comfort within a reasonable range.

The purpose of the present study is to develop suitable LiCl/LiBr–zeolite composite adsorbents for TCHS applications and to perform test of the thermal storage performance in a lab-scale adsorption heat storage reactor. Finally, TRNSYS was used to evaluate the heating effect of this system. The studied pure zeolite and composite adsorbents were subjected to electron microscopy measurement, kinetic adsorption performance and DSC tests to investigate their pore characteristics, water adsorption, heat transfer and mass transfer properties. Based on the identified optimal LiCl/LiBr–zeolite composite adsorbent, a set of adsorption heat storage test rig was constructed. Considering the effects of both air flow rate and air humidity, the water adsorption performance of the developed composite adsorbent under different operating conditions was explored, and the energy storage density and cycle stability of the material were also obtained and analysed. Although the heat storage performance of the open system TCHS has received more attention, the performance of the combination of solar thermal collection and TCHS system heating to meet the space heating needs is still less researched. In this study, a simulation model of the dwelling was developed in Trnsys software. In the winter climate environment, the reactor is charging by solar panels during the day, and discharging by hydration reaction of the adsorbent in the reactor during the night. The heat released is used for space heating of the house to maintain the room temperature in the range of  $21 \pm 1$  °C. When the material reaction completely stops exothermic, start gas as auxiliary energy supplement, continue to heat the house. This paper also simulates a reference system with gas as the heating energy source. The heating effect of the TCHS system with a time period of 7 months was studied. Analyze and calculate gas energy savings to assess the benefits of the system.

## 2. Materials

### 2.1. Preparation of Composite Adsorbent

Anhydrous LiCl and anhydrous LiBr were respectively purchased from Sinopharm Chemical Reagent Co., Ltd., (Shanghai, China). and Hefei BASF Biotechnology Co., Ltd., (Hefei, China). 3A zeolite was purchased from Clear Spring Technology Co., Ltd., (Singapore).

Figure 1 shows the preparation process of the composite adsorbent. First, anhydrous LiCl and anhydrous LiBr solids with pre-defined mass ratio (1:1 to 1:5) were separately added to distilled water and continuously mixed to allow the salt powder to completely dissolve in the water to ensure uniform mixing with the 3A zeolite. To determine the optimal ratio for a composite adsorbent, five salt solution groups with various mass fractions (5 wt%, 10 wt%, 15 wt%, 20 wt% and 25 wt%) were prepared. Considering the reasonably cost effective and easy in process, this study used the water impregnation method to manufacture the composite adsorbent, which can achieve the desired effect

of zeolite loading salt. In the first step, zeolite spheres of 3–5 mm size were soaked in deionised water for 12 h for pre-treatment; after soaking, the zeolite was heated and dried at 200 °C for six hours before being cooled. The second step involved impregnating the previously treated dry zeolite with salt solution. 30 g of zeolite was soaked in 50 g of salt solution. To ensure that liquid solution was evenly filled in the pores of zeolite, this impregnation process was conducted with continuous stirring using a glass rod. Finally, the salt solution-carrying zeolite was dried again in an oven at 200 °C to form a dehydrated composite adsorbent. The samples were numbered Z0 (pure zeolite) and Z5, Z10, Z15, Z20 and Z25 for the samples using 5–25 wt% salt solution (e.g., Z5 corresponds to the composite adsorbent manufactured using 5 wt% salt solution). The ingredient with various ratios of the manufactured composites are shown in Table 1. Notably, it was found during the preparation that salt concentrations above 25 wt% were not easily made into composite adsorbents. The structure of zeolite particles is destroyed during the impregnation process, and some of the zeolite particles will be completely broken into powder form. Their performance was tested to be inferior to that of the intact sample set, so the maximum concentration of salt solution used in this experiment was 25 wt%.

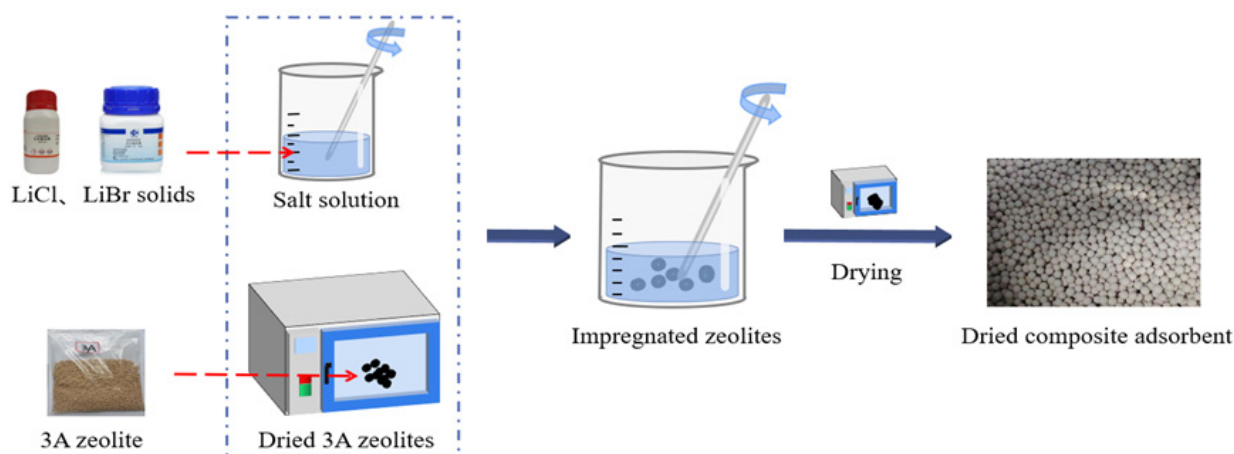


**Figure 1.** Preparation process of the composite adsorbent.

**Table 1.** The ingredient with various ratios of the manufactured composites.

No.	Z0	Z5	Z10	Z15	Z20	Z25
Salt solution concentration	0 wt%	5 wt%	10 wt%	15 wt%	20 wt%	25 wt%
LiCl:LiBr mass ratio	-	1:1	1:2	1:3	1:4	1:5

## 2.2. Properties of the Composite Adsorbent

### 2.2.1. Morphologies

The samples were imaged using a Sigma 300 model scanning electron microscope (SEM). Figure 2 shows the microscopic surface morphology of the samples at a magnification of 20,000 $\times$ . As shown in the Figure 2a–f, the pure zeolite (sample Z0) exhibits clear pores, while the remaining samples demonstrate that the salt and 3A zeolite are well mixed, with salt tending to collect in the uneven areas of the zeolite surface. As the salt content of the composite increases, they gradually adhere to the surface, thereby increasing the surface roughness. The surface of the adsorbed sample displayed clear salt crystallisation, with increased crystallisation observed with increasing salt concentration. Such a phenomenon is consistent with previous descriptions of the microstructure of adsorbents loaded with salts. The outer surface of sample Z25 was almost completely covered with salt crystals, however, the channels leading from the surface of the zeolite to its core were unobstructed. More salt loading can increase the water adsorption capacity because salt embedded in the sample creates numerous micropores; this process significantly increases the surface area

of the composite material and the extent of its contact area with water vapour. However, high-concentration salt solutions are also susceptible to crystallisation, which may limit the material's mass transfer capacity. It is therefore essential to identify the optimum concentration of salt solution used for manufacturing the composite adsorption material.

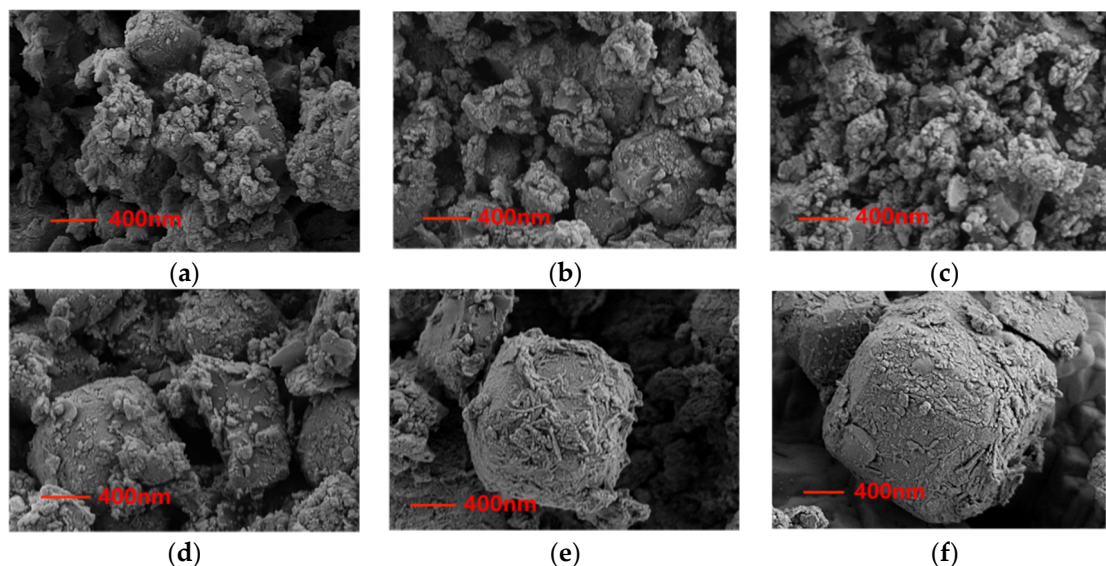


**Figure 2.** SEM photos of the composites with different solution concentrations at the magnification of 2000 times: (a) Z0; (b) Z5; (c) Z10; (d) Z15; (e) Z20; (f) Z25.

### 2.2.2. Pore Properties

The pore volume and pore size distribution of the materials were examined by a fully automatic surface and pore size analyzer (BET, Micromeritics APSP2460) using nitrogen adsorption-desorption method. The pore size distributions and specific surface areas of porous materials were calculated using the Barrett-Joyner-Halenda (BJH) theory and the Brunauer-Emmet-Teller (BET) theory. The porous properties of the samples, such as pore size distribution, pore volume and surface area, are listed in Table 2. Figure 3a,b show the pore volume versus different pore widths. A sufficiently large pore volume can maintain the passage of water vapor in and out of the adsorption process. Otherwise, the mass transfer of water adsorption kinetics would be limited. All samples showed a similar trend, increasing rapidly at the beginning and stabilizing at the end. They all had a peak in pore volume at about 5–7 nm pore width, which means that most of the pore sizes were distributed in this range. Moreover, the pore volume or average pore size may decrease as the concentration of the solution increases. Although a high salt concentration theoretically provides more reactants for water adsorption, it also limits water adsorption by sacrificing some mesoporous mass transport channels in the support structure. This suggests that the balance between LiCl/LiBr loading and pore volume in the composite should be carefully maintained to accomplish an optimal thermochemical thermal storage material.

**Table 2.** The essential porous characteristics of the manufactured composite adsorbents.

Group	Surface Area (m <sup>2</sup> /g)	Pore Volume (cm <sup>3</sup> /g)	Adsorption/Desorption Average Pore Diameter (nm)
Z0	27.73	$6.36 \times 10^{-2}$	9.02/10.71
Z5	28.11	$6.22 \times 10^{-2}$	8.74/10.41
Z10	28.76	$6.35 \times 10^{-2}$	8.65/10.21
Z15	26.90	$6.07 \times 10^{-2}$	8.89/10.53
Z20	25.67	$5.88 \times 10^{-2}$	9.00/10.84
Z25	25.83	$5.83 \times 10^{-2}$	8.86/10.63

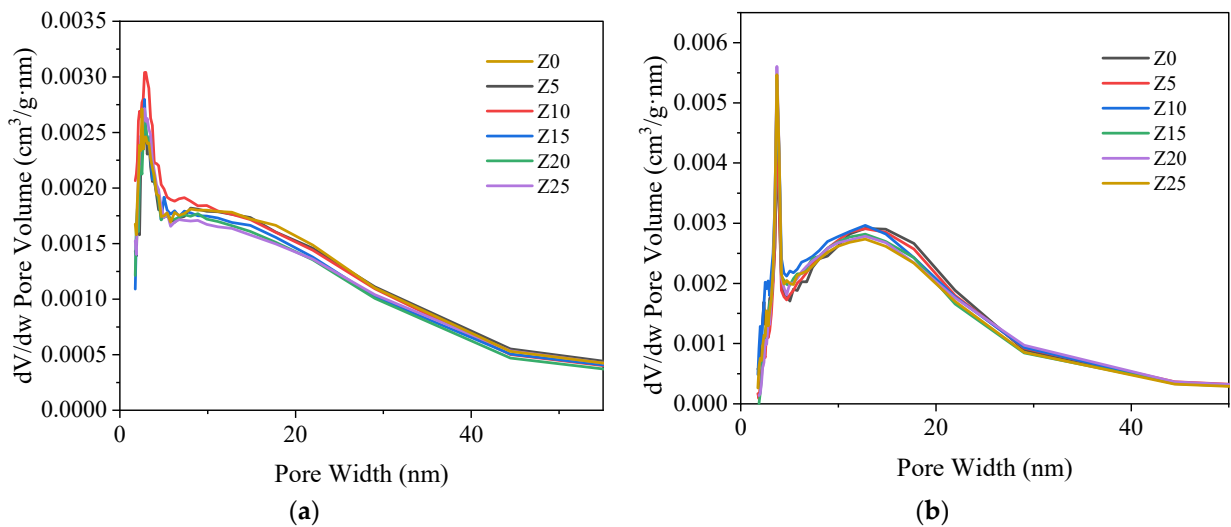


**Figure 3.** BET results of the prepared composite adsorbents. (a) Adsorption pore volume vs. pore width, (b) Desorption pore volume vs. pore width.

### 2.2.3. Adsorption Kinetic Performance

The adsorption rate and capacity of water vapour have significantly impact on the energy storage capacity of LiCl-LiBr-zeolite adsorption systems. The adsorption tests were conducted in a constant temperature and humidity chamber (climatic chamber) under a temperature of 25 °C and relative humidity (RH) levels of 60%, 70%, 80%, and 90% to analyse the adsorption kinetics. The mass change of the adsorbent samples over 24 h was measured by using an electronic balance. The water uptake kinetics of samples are depicted in Figure 4. When the weight difference is below 5% in two consecutive 60 min intervals, adsorption equilibrium was deemed to have been achieved.

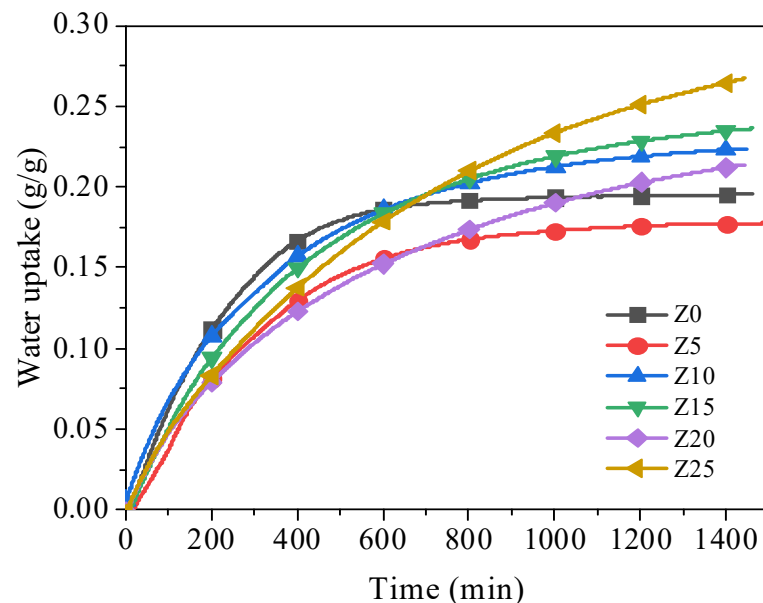


**Figure 4.** Water adsorption kinetics of samples with different composites.

The pure zeolite, Z0, exhibits high adsorption rate at the early adsorption stage, reaching a maximum value of 0.18 g/g after 600 min of adsorption at 25 °C and 80% RH, as shown in Figure 4. Comparing to Z0, Z5 performs more poorly as an adsorbent with lower adsorption rate and capacity, which is due to its low salt content and partially blocked

water transfer channels. Higher salt content adsorbents take longer to achieve equilibrium, suggesting that the water transfer channels were blocked more significantly with increasing salt content; however, the adsorption rate are larger at late stage of adsorption and the final adsorption capacity is also promoted. In contrast, samples Z10, Z15 and Z25 demonstrate reasonable adsorption rates and capacities. However, the salt swells upon hydration, leading to the blockage of the zeolite pore channels, especially in Z20 as shown in BET result (Table 2). Both the active adsorption area (specific surface area) and the mass transfer channel (pore volume) were reduced. This self-clogging effect is detrimental to the water adsorption behavior of the material. Thus, Z20 exhibited a refrained adsorption rate than other candidates until 700 min due to the corresponding significant mass transfer barrier; thereafter due to the enhanced water adsorption capacity, i.e., increased salt loading, the overall water adsorption capacity is higher than Z0 and Z5. Finally, the adsorption capacity of Z10, Z15 and Z25 are 0.22 g/g, 0.24 g/g and 0.27 g/g, respectively. Z15 always maintains a high adsorption rate and has a high adsorption capacity when the adsorption equilibrium is reached.

The RH significantly impacts the equilibrium adsorption capacity of every sample. Figure 5 shows the adsorption capacity of the samples after reaching equilibrium at 40%, 60% and 80% RH. The overall pattern indicates that high RH encourages water vapour adsorption, thus increasing the adsorption capacity of all samples. This occurs because the increased RH elevates the water vapour pressure difference between the water vapour in the air and the equilibrium water vapour pressure of the adsorbent material, which facilitates the effective diffusion of water vapour into the adsorbent. Another significant factor is that salt deliquescence in a high-humidity environment reduces zeolite micropore blockage, which is advantageous for increasing water adsorption. Nevertheless, the swelling of salt hydration occurs at the same relative humidity conditions, which may lead to the clogging of zeolite pores. The blocking extent referring to the solution concentration was partly revealed in the BET result, which has been discussed in last section.

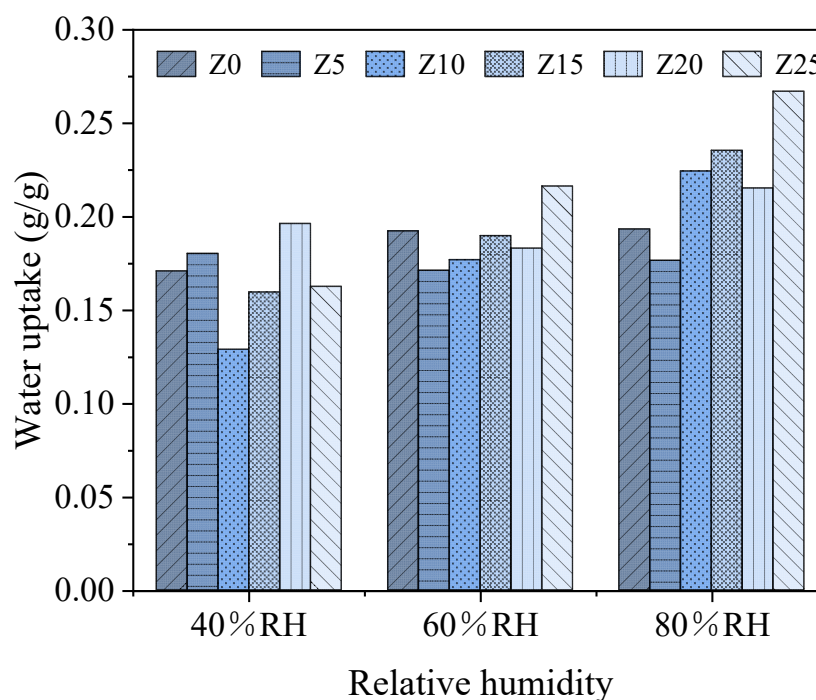


Figure 5. Water adsorption capacity with different relative humidities.

#### 2.2.4. Adsorption Heat

Differential scanning calorimetry (DSC) were performed on Z0 to Z25. Using a simultaneous thermal analyser, with  $N_2$  selected as the test atmosphere. The experimental

temperature conditions were set to increase from 30 °C to 300 °C, the heating rate was 5 °C/min, and the experimental time was 1 h. The heat flow was recorded throughout the process.

The DSC curves of the endothermic dehydration process of each group of samples are shown in Figure 6a. The theoretical heat storage density of the composite heat storage material is obtained by integrating the curve inland in a certain range, and plotted in Figure 6b. Sample Z0 exhibits a heat storage density of 447.1 J/g; however, in all instances, the heat storage density of the composites are higher than that of the pure zeolite. This effect is due to the contribution of salt to the water absorption capacity, thereby increasing its thermal storage density. The most significant thermal storage density is recorded in Z5 (32.6% higher than Z0). Although no positive correlation was identified between the heat storage density of the composite adsorbent and the salt solution concentration, a higher solution concentration may nonetheless hinder mass transfer during water adsorption, thus resulting in a lower heat storage density. Therefore, samples Z5, Z10 and Z15 can be used as the three ‘ideal’ samples for the analyses in this study because their heat storage densities do not markedly differ.

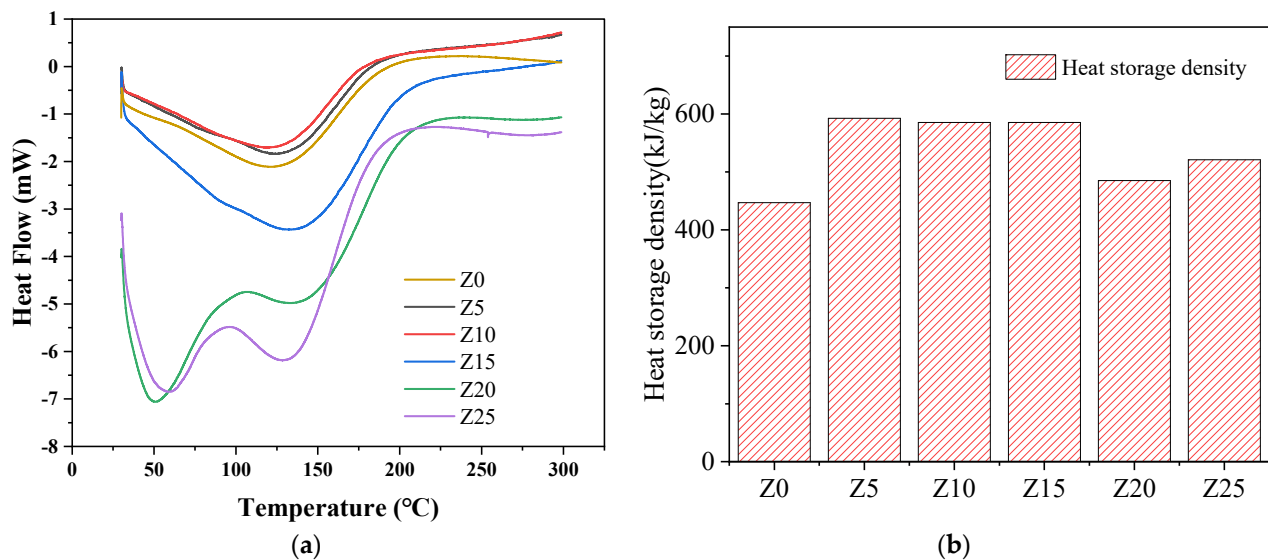


**Figure 6.** DSC results of the prepared composite adsorbents. (a) Heat flow curve, (b) Heat storage density.

### 2.3. Selection of the Optimal Adsorbent

Based on the analyses above, the adsorption performance of composite materials are found to be variably impacted by the salt concentration with no clear linear relationship. As confirmed by the SEM experiments, changing the salt content influenced the microscopic scale size characteristics of the composite adsorbent. The investigation of the adsorption kinetics of the samples revealed that Z15 had both a high water adsorption rate and capacity. Further DSC studies show the heat storage density of Z15 is up to 585.3 J/g, which is 30.9% higher compared to Z0. On this basis, sample Z15 was selected as the optimal composite adsorbent for lab-scale open system experiment.

## 3. Experiment Overview

### 3.1. Test Rig

Figure 7a shows a schematic diagram of a reaction system. Figure 7b is the photo of the thermochemical heat storage reaction system, which comprises a pipe with a valve, a fan, a humidifier and a reactor. The reactor is placed inside the hollow cylindrical pipe that houses the entire apparatus. The rightmost side of the pipe is connected to an inclined flow booster pipe fan. In addition, the humidifier is connected to the inlet air duct. The layout of the reactor is shown in Figure 7c. The wire mesh container containing the composite

adsorbent Z15 is covered with a metal disc-shaped covering. To achieve a more thorough and uniform adsorbent reaction, the reactor is fitted with a thin tube with perforations in the centre shaft. In total, 3 kg of Z15 adsorbent was placed inside the reactor. During the experiment, the pipes were covered in aluminium foil insulation foam to minimize heat loss to the exterior. Temperature and humidity sensor (A-Pt100) were installed at the inlet and outlet of the reactor to measure the temperature and humidity of the air. To assess the volume of air passing through the pipe, a gas flow meter was installed at the end of the pipe.

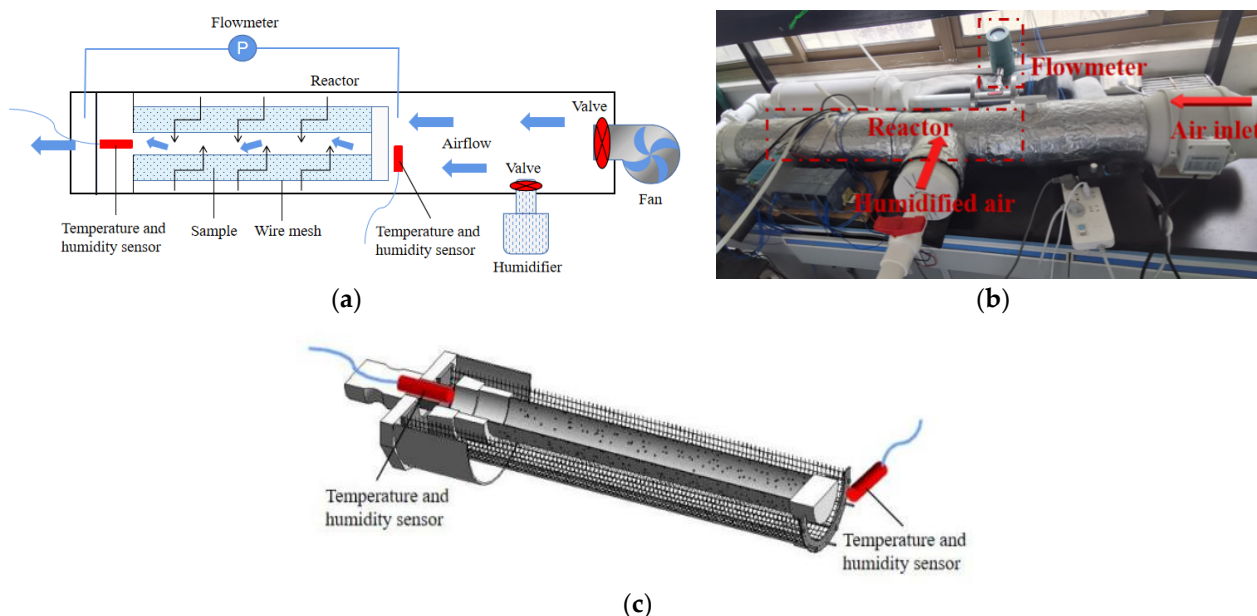


**Figure 7.** Adsorption experimental pipeline diagram: (a) piping schematic diagram; (b) reaction system assembly diagram; (c) reactor cross-sectional view.

### 3.2. Experimental Procedures

In this study, the air flow rate and relative humidity were chosen as the main variables for investigation; thus, to examine the impacts of both on the thermal storage performance of the composite salt, orthogonal experiments were configured with airflow rates of 5 m<sup>3</sup>/h, 10 m<sup>3</sup>/h, 15 m<sup>3</sup>/h and 20 m<sup>3</sup>/h and humidity levels of 60%, 70%, 80% and 90% RH.

The 3 kg of LiCl/LiBr-zeolite composite thermal storage material was placed in the reactor, and the fan and humidifier were adjusted to ensure that the experimental conditions were within the predetermined ranges. Overall, the adsorption reaction procedure for the composite material takes 12 to 20 h to complete. In the initial stage of the reaction, the outlet temperature rises at a certain rate and then begins to fall after reaching its peak. The temperature curve subsequently tends to slowly level off and return to the inlet temperature, indicating the reaction's completion. The adsorption material in the reactor was heated in an oven following each experiment, totally dehydrated, and then cooled in preparation for the following experiment.

### 3.3. Energy Density Calculate

For the thermochemical heat storage system, the energy density is a crucial indicator to evaluate the performance of the composite salt heat storage, which can be calculated by the following equation. Since the humidity data measured by the temperature and humidity sensor is 0–100% RH, the water vapor partial pressure  $P_v$  in the wet air can be obtained by the following Equation (1) [50]:

$$P_v = \phi P_s \quad (1)$$

$P_s$  is the saturated water vapor partial pressure [50], and the absolute humidity  $d$  of wet air can be expressed as:

$$d = 0.622 \frac{P_v}{P - P_v} \quad (2)$$

The enthalpy  $H$  of wet air can be calculated from Equation (3) [39]:

$$H = 1.005t + d(2500 + 1.84t) \quad (3)$$

The energy storage density  $Q_E$  can be calculated by Equation (4) [51]:

$$Q_E = \frac{\int_0^{t_d} \rho_f q_v (H_{exit} - H_{inlet}) dt}{M} \quad (4)$$

$\rho_f$  is the density of the dry air,  $q_v$  is the volume flow rate of the gas,  $M$  is the total mass of the adsorbent material in the reactor, this experiment uses  $M = 3$  kg.

The energy discharge efficiency of this reactor can be estimated using Equation (5) [39]:

$$\eta = \frac{Q_E}{Q_D} \times 100\% \quad (5)$$

$Q_D$  is the theoretical heat storage density of the composite adsorbent, which is derived from the DSC experiment in Section 2.2.3.

## 4. Experimental Results and Discussion

### 4.1. Effect of Air Flow Rate

For each of the four relative humidity levels, Figure 8 illustrates the impact of various air flow rates on the exit air temperature. All the temperature differential variations in Figure 8 initially climb rapidly and then slowly decline until the temperature rise becomes close to zero. The final temperature increase reduces to zero at the point of which the adsorbent is saturated, the stored heat is completely released and the reaction is over. The rate of temperature rise increases with increasing air flow rate, with the recorded temperature rise rate at a flow rate of  $5 \text{ m}^3/\text{h}$  noticeably lower than the other measured flow rates. Since the air flow rate affects the rate of moisture transfer and the low air flow rate limits the process of mass and heat transfer between the wet air and the adsorbent [52]. However, the effective reaction time of the material becomes longer at low flow rate conditions. The reaction time decreases consistently with increasing flow rate under conditions of 60% RH. The adsorbent still tends to have a shorter reaction time at high flow rates when the air has an RH of 70% or below, as shown in Figure 8a,b, however, as the relative humidity rises, this difference becomes less noticeable at flow rates of  $10 \text{ m}^3/\text{h}$ ,  $15 \text{ m}^3/\text{h}$ , and  $20 \text{ m}^3/\text{h}$ , as shown in Figure 8c,d.

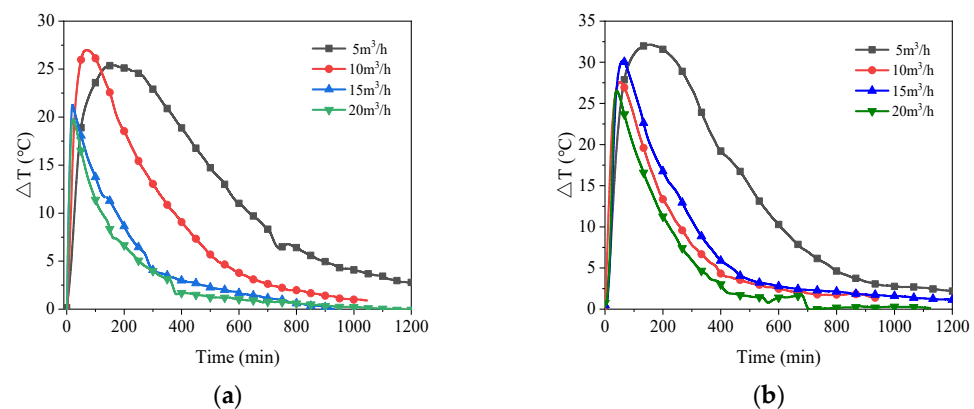
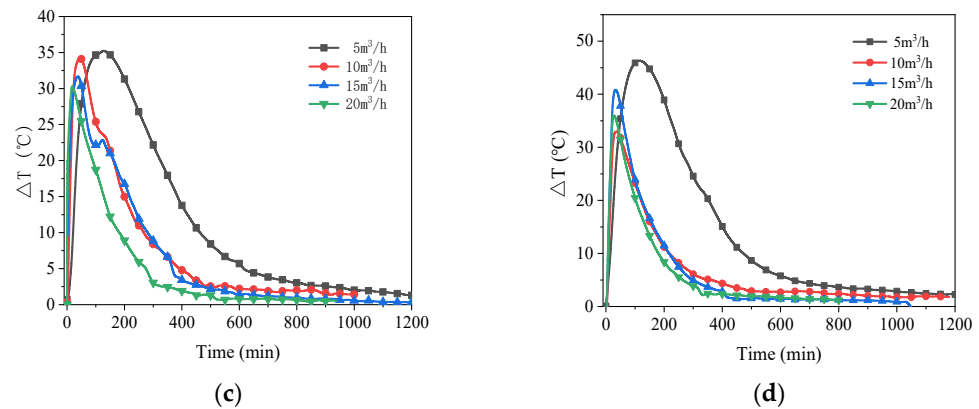


Figure 8. Cont.



**Figure 8.** Air temperature rises with time for different air flow rates at four air relative humidity: (a) 60%RH; (b) 70%RH; (c) 80%RH; (d) 90%RH.

#### 4.2. Effect of Air Relative Humidity

As the results from Figure 9, the maximum temperature difference increases as the relative humidity increases. The air temperature increased by 84.1%, 28.1%, 93.3%, and 79.8%, respectively, when the relative humidity was elevated from 60% to 90%. Similarly, when more humid air flowed through the reaction pipeline, the rate of temperature rise of the air at the initial stage was higher. This behaviour was especially noticeable at a flow rate of 5 m<sup>3</sup>/h. It is because that the high relative humidity provides higher pressure difference to drive the adsorption reaction, which accelerates the hydration reaction of the material driving the heat generation. This causes the increase in temperature rise value and rate.

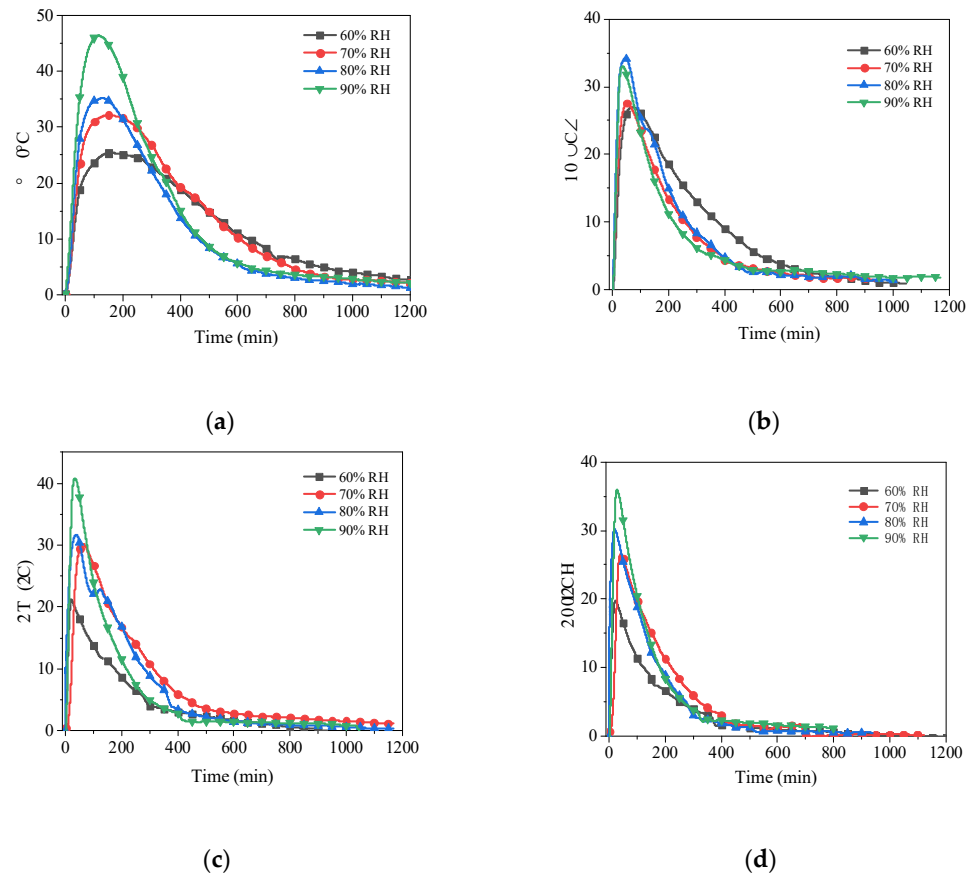


**Figure 9.** Air temperature rises with time for different air relative humidity at four air flow rates: (a) 5 m<sup>3</sup>/h; (b) 10 m<sup>3</sup>/h; (c) 15 m<sup>3</sup>/h; (d) 20 m<sup>3</sup>/h.

#### 4.3. Energy Storage Density

For each group of experiments, the energy storage density was calculated and plotted in Figure 10. It can be seen from the experimental results that the maximum temperature difference and the temperature rise rate have a positive correlation trend with the gas flow rate and relative humidity. However, energy storage density does not have such a law. From the formula, it shows that the energy storage density is not only related to the maximum temperature difference, but also to the effective reaction time. In addition, it cannot be ignored that in the same room temperature environment, the heat loss under different experimental conditions is different. The higher the flow rate, the more heat is lost through the pipe, metal reactor. In this experiment, the composite material has the highest heat release value of 434.4 J/g when the gas flow rate is 15 m<sup>3</sup>/h and the relative humidity is 70%, and its energy discharge efficiency is 74.3%.

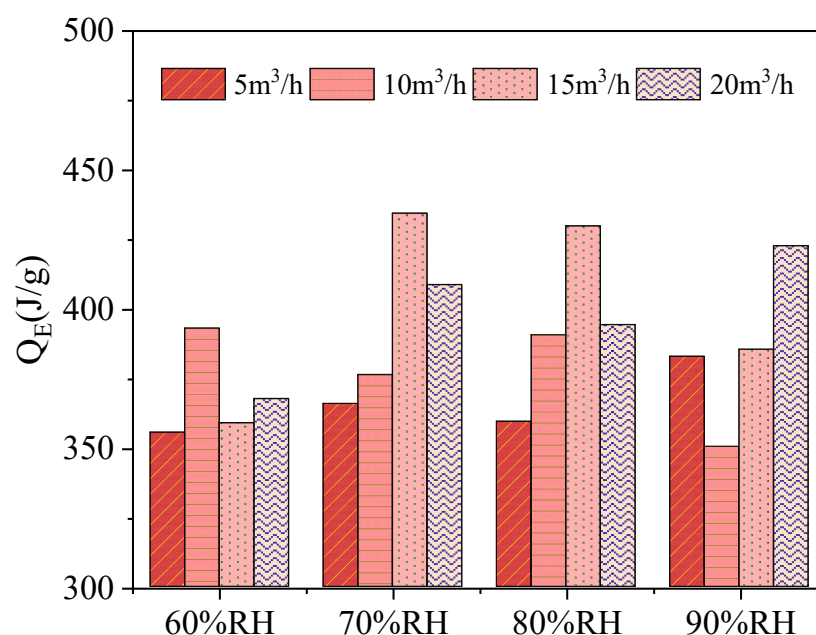


Figure 10. Energy storage density with different experimental conditions.

#### 4.4. Cyclic Experiments

To get the cyclic performance, the adsorbent material was subjected to ten cycles of adsorption/desorption under experimental conditions with an air flow rate of 15 m<sup>3</sup>/h and a relative humidity of 70%. Figure 11 shows the variation of the outlet temperature with time. It can be seen that the rate of temperature increase decreases with the number of cycles. Figure 12 shows the variation of the energy storage density for the ten cycling experiments. The average error of the cycling result was 0.41%, which proved the experimental result to be convincing. Although the adsorption heat decreased significantly after the first three trials (by 0.53%), the decrease slowed down in the subsequent studies, with a final rate of change of only 0.17%. This indicates that while certain microstructure changes do occur in the composite adsorption material during cycling, these changes become smaller and smaller as the number of cycles increases. Cycling experiments show that this material can be recycled for a long time in cross-season heat storage.

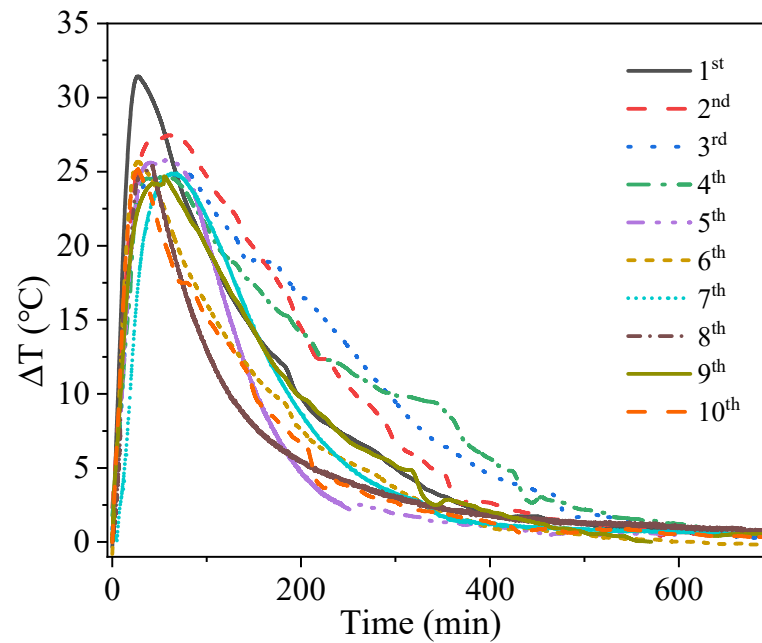


Figure 11. Air temperature rises with time for cyclic experiments.

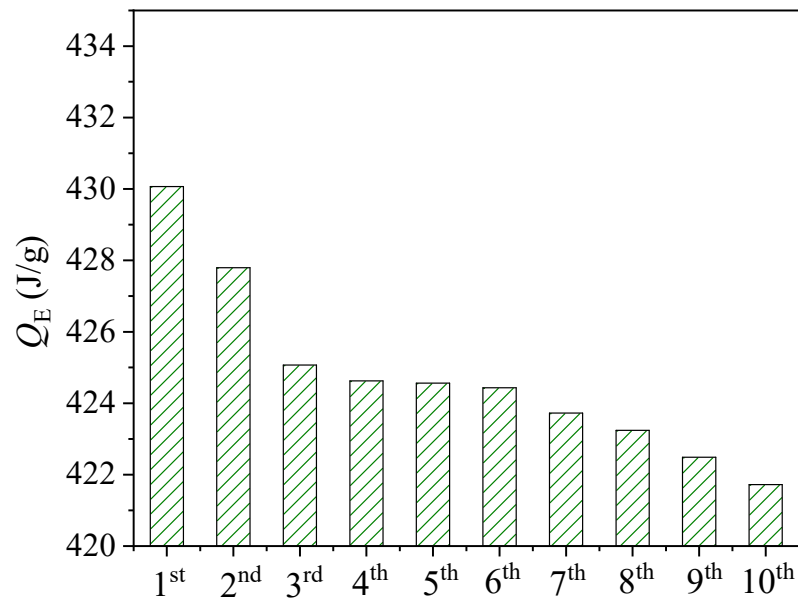


Figure 12. Energy storage density for cyclic experiments.

## 5. Numerical Simulation

### 5.1. System Description

In this study, the TRNSYS software was used to dynamically simulate the charging mode and the discharging mode. The system mainly consists of three parts. The first part is solar energy collection and energy storage; the second part is the reactor heat release as well as gas heating; the last part is the residential model as the heated unit. Figure 13 shows the charge mode and discharge mode for the entire operation. During the day, the sorbent is heated and dehydrated by a solar-triggered charging mode. All heat is stored, and there is no heat loss in this process (the heat conversion efficiency is 74.3%). The input heat from the solar panels regenerated the adsorbent in the reactor. At night, the discharge mode is triggered by blowing air at a certain flow rate and humidity into the reactor. All the heat of adsorption released by the reactor heats the air, which is mixed with ambient air and passed

into the dwelling to heat the space. The specific content of the heat release analysis module is described in Section 3. The optimal heat extraction efficiency based on experimental data converts the energy stored during the day. In addition, gas is used as an auxiliary energy to supplement the insufficient power required by the house. Considering real life, assume that a simple thermostatic controller is used to maintain the indoor temperature at  $22 \pm 1$  °C. When the indoor average area temperature is lower than 21 °C, the fan starts to work, and the reactor provides heat; when it is higher than 23 °C, the fan stops running. In addition, when the reaction of the adsorbent in the reactor is no longer enough to supply the indoor temperature to 20 °C, no heat is provided, and the gas is started for heating work.

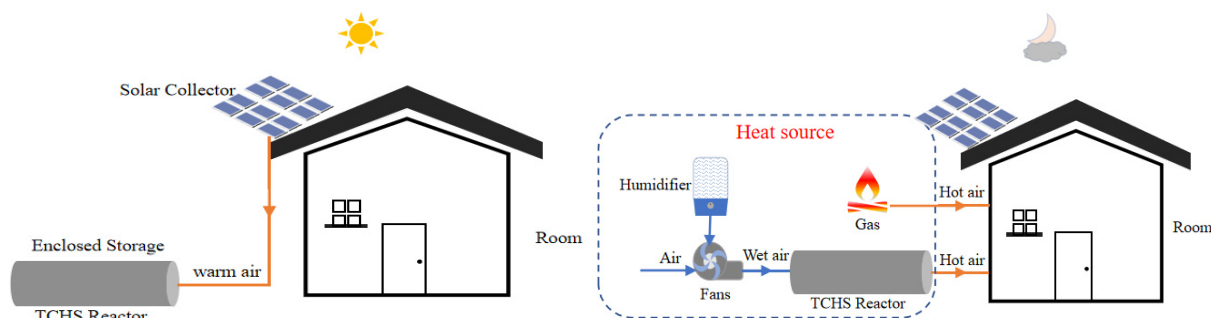


**Figure 13.** Charge and discharge modes of an open TCHS system.

To realize the residential model of the study, the 3D architectural design software SketchUp was used. A typical two-story residential model (actual size is 6150 mm × 8350 mm × 4550 mm). As shown in Figure 14, the house model is then imported into TRNSYS through the TRNSYS 3d plugin. Next, transfer the module in TRNSYS Simulation Studio to build the TCHS-building simulation platform. Figure 15 shows the dynamic simulation flow, with controllers for each zone. Table 3 gives the structural information of the building used to determine the parameters of the walls, roof, floor and windows. The TRNSYS program generally creates a flexible environment for modelling buildings, where different building descriptions can be obtained by changing design parameters. However, this study mainly focuses on the performance research of the TCHS system. It explores the degree of its effect applied to the building, so that the parameter setting of the building itself is not changed. The system lays half-roof synchronous monocrystalline silicon solar modules and uses Type103 modules to simulate the photovoltaic power generation process. The conversion efficiency of this component can reach 21.3% under standard test condition. The climatic conditions entered refer to the climatic data of a typical weather year in Newcastle, including ambient temperature, instantaneous solar radiation on the horizontal plane, wind speed, and ambient air relative humidity. In the control module of the software, temperature control, time control and heat control are adopted. At the same time, the indoor temperature is within the range of  $22 \pm 1$  °C, and the TCHS heating working time is from 20:00 at night to 9:00 in the morning of the next day. During this time period, when the room needs heating and the energy storage of the TCHS system is not exhausted, the system heats the room. The hot air leading to the room is distributed according to the area ratio of each room. In the analysis process of building energy consumption, the Type56 analysis module is used. The terminal calls the multi-region building model TRNBUILD to simulate the thermal process of the room. By simulating, the domestic temperature, the data of photoelectric conversion and energy consumption are calculated. The above data are monitored by the Type65 online plotter and monthly statistical output by Type46. The simulation time step is 0.05 h, and the simulation period is from October to April of the following year when heating is required.

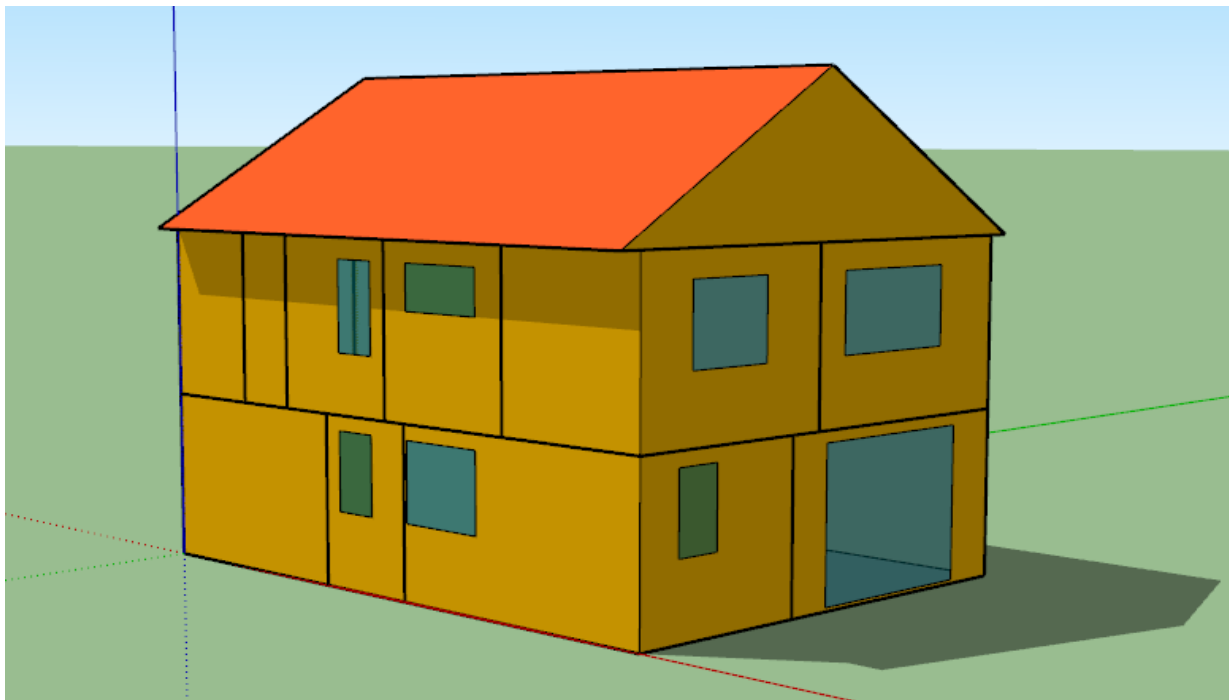


Figure 14. 3D model of the building.

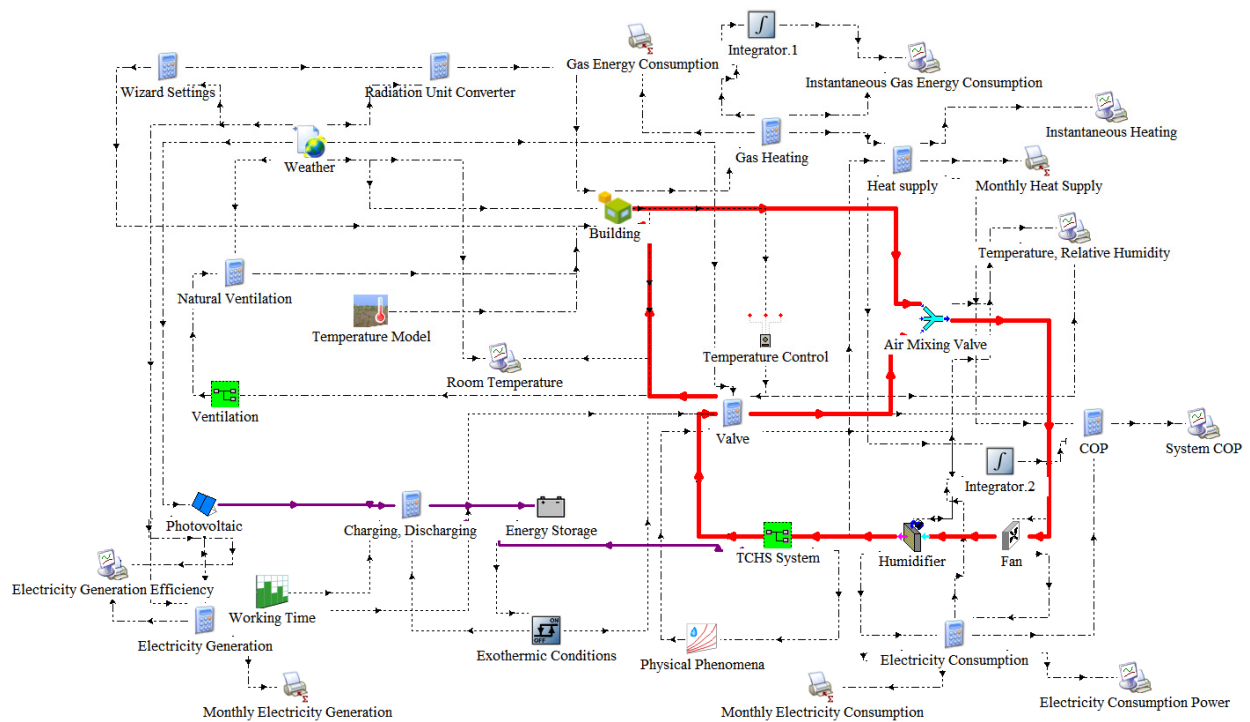


Figure 15. TRNSYS model for building with TCHS system.

**Table 3.** Physical and thermal properties of building materials used in modelling using TRNSYS.

Surfaces	Thermal Properties
Doors	U = 2.82 W/m <sup>2</sup> ·K Longwave emission coefficient = 0.9 Convection coefficient = 11 kJ/h·m <sup>2</sup> ·k (inside), 64 kJ/h·m <sup>2</sup> ·k (outside)
Windows	U = 1.27 W/m <sup>2</sup> ·K g-value = 0.74 coefficient = 11 kJ/h·m <sup>2</sup> ·k (inside), 64 kJ/h·m <sup>2</sup> ·k (outside)
Floors	U = 0.25 W/m <sup>2</sup> ·K Solar absorptance = 0.8 Longwave emission coefficient = 0.9 Convection coefficient = 11 kJ/h·m <sup>2</sup> ·k
Walls	U = 0.54 W/m <sup>2</sup> ·K Solar absorptance = 0.7 Longwave emission coefficient = 0.9 Convection coefficient = 11 kJ/h·m <sup>2</sup> ·k
Roof	U = 2.69 W/m <sup>2</sup> ·K Solar absorptance = 0.8 Longwave emission coefficient = 0.9 Convection coefficient = 11 kJ/h·m <sup>2</sup> ·k (inside), 64 kJ/h·m <sup>2</sup> ·k (outside)

## 5.2. Performance Analysis

### 5.2.1. Evaluation Indicators

Compared with the energy consumption  $Q_1$  of the traditional (gas) system, the energy consumption  $Q_2$  achieved by the retrofitted system (TCHS and gas) is calculated according to the following Equation (6) [53].

$$Q_2 = 2.42 \times (Q_{\text{hum}} + Q_{\text{fan}}) + Q_{\text{gas}} \quad (6)$$

The heating of TCHS requires raw power from fans and humidifiers.  $Q_{\text{hum}}$  and  $Q_{\text{fan}}$  represent the power consumption of the humidifier and fan, respectively, and  $Q_{\text{gas}}$  is the gas consumption. Among them, 2.42 is the energy conversion factor of electricity equivalent to primary energy. For TCHS systems, the average heating situation is expressed using the coefficient of performance  $COP$ , which is defined as [54]:

$$COP = \frac{Q_{\text{sor}}}{Q_{\text{hum}} + Q_{\text{fan}}} \quad (7)$$

Among them,  $Q_{\text{sor}}$  provides heat for the TCHS system. It can be calculated from the heat capacity obtained by air flowing through the adsorbent material.

### 5.2.2. Analysis of Residential Heating Performance Based on TCHS System

The dynamic simulation of the charging and discharging process of the established system is carried out for a period of 7 months. The results show the operating state and performance of the system under various climatic conditions. Figure 16 shows the changes in ambient temperature and room temperature during the simulation cycle. Although there is temperature control to set the temperature in the range of  $21 \pm 1$  °C, it can be seen that the overall trend is still affected by the ambient temperature.

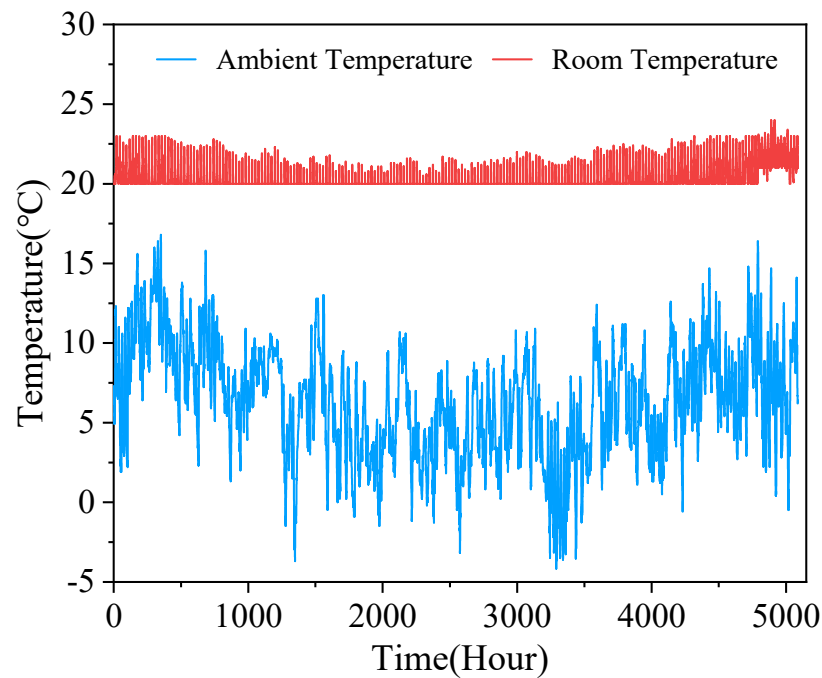


**Figure 16.** Variation of ambient temperature and room temperature under simulation cycle.

Figure 17 shows the solar power generation, the heat of desorption  $Q_{des}$  of the adsorbent and the heat of adsorption  $Q_{sor}$  of the adsorption system for each month in charge mode and discharge mode. As the climate temperature rises, the better the solar heat collection effect is, the more energy can be provided to the adsorption heat storage system, and the better the effect of the adsorption heat supply. The conversion efficiency between the two follows the experimental results in Section 4.3, which is close to the optimal energy conversion efficiency of 74.3%.

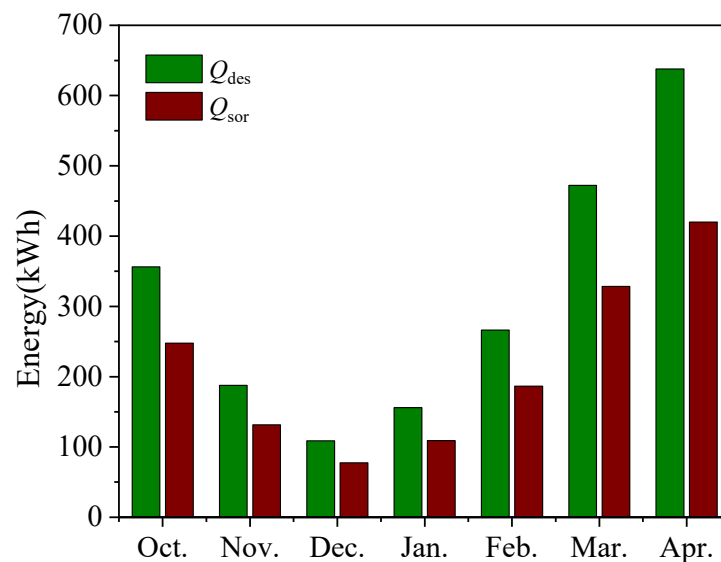


**Figure 17.** Monthly change in thermal capacity.

To evaluate the energy consumption reduction of the heating system by the heat release of TCHS. Figure 18 plots the energy consumption  $Q_1$  of gas heating alone, and the energy consumption  $Q_2$  of the adsorption system and gas co-heating. It can be seen from the figure that the TCHS system can reduce the consumption of gas, and the total energy consumption in seven months can reduce the gas consumption by 8.8%. However,

natural gas still accounts for most energy consumption, as TCHS is limited by solar energy harvesting. After the TCHS releases all the heat of adsorption, the fans and humidifiers stop working. If the ability to increase the TCHS reserve solar energy is improved, the heat release from TCHS can be increased. The power consumption of fans and humidifiers accounts for the central part, which is expected to save most of the gas.

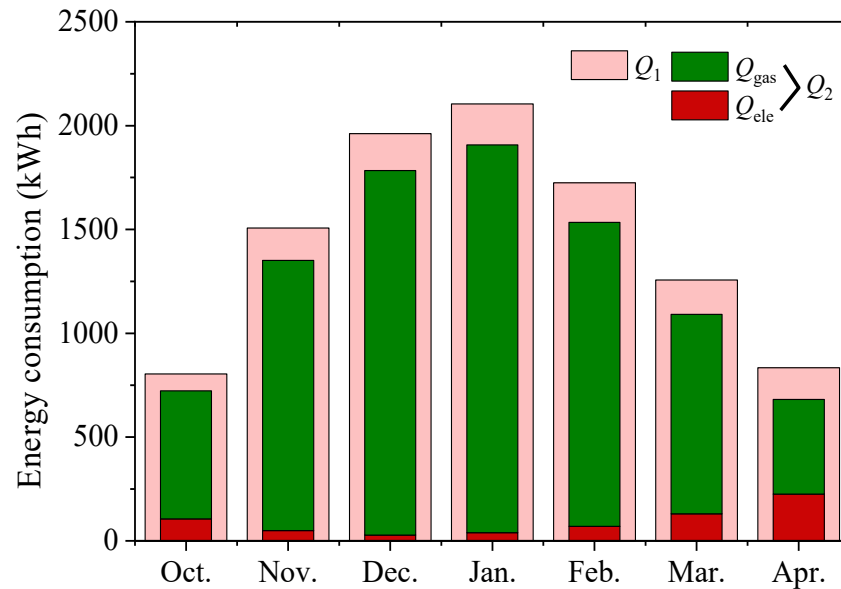


Figure 18. Monthly energy consumption of the system.

Figure 19 plots the *COP* values for TCHS for each month. The maximum was in December at 6.67. This is because the TCHS system relies on the hydration reaction of the adsorbent, which is affected by the climatic environment. Because the air humidity in Newcastle in December is relatively high, it can provide natural moisture for the reaction of the TCHS system, reducing the burden of electricity consumption of the humidifier. Similarly, the minimum value of 4.48 appeared in April. Although solar energy was abundant in April, the charging capacity reached the maximum (Figure 17); but the natural air was dry, which significantly increased the power consumption of the humidifier (Figure 18). The average monthly *COP* was calculated to be 5.56. If the investment in the TCHS system is increased, it is likely to replace most of the gas, and the heating demand of the house can be met with less power consumption.

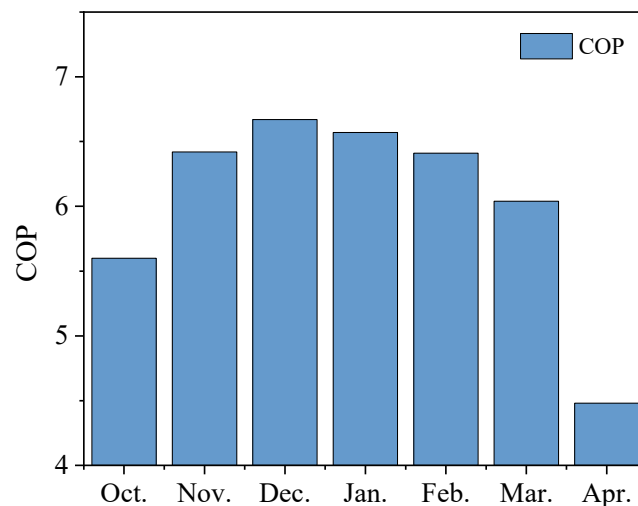


Figure 19. Monthly COP of TCHS system.

## 6. Conclusions

In this study, a LiCl/LiBr–zeolite composite adsorbent was developed. Subsequently, it was applied to a lab-scale reaction unit for experimental study. For the further evaluation of the practical building heating performance of TCHS system, it was applied to the domestic house. The TCHS-building model was built in the TRNSYS program. The main conclusions are as follows:

- The different salt concentrations resulted in different adsorption capacities and thermal storage properties. Under the same experimental conditions, composite Z15 shows the best adsorption performance.
- In the adsorption heat storage experiment using a lab-scale reactor, the temperature rise rate at the outlet of the reactor is influenced by the air flow rate and humidity. The studied composite adsorbent exhibited its highest heat density of 434.4 J/g at an air flow rate of 15 m<sup>3</sup>/h and an RH value of 70%, achieving an energy discharge efficiency value of 74.3%.
- The average error of 10 cycles repeating adsorption experiment was 0.41%. The decrease in temperature lift and adsorption heat showed a slowing down trend with the number of cycling experiments, and the heat density of the last cycle test decreased by only 0.17% which indicated a good periodicity and stability of composite adsorbent.
- The TRNSYS simulation found that the heating effectiveness of the TCHS system is dependent on the ambient temperature and humidity, and that the power consumption (i.e., fans and humidifiers) is lower in December, reaching a maximum COP of 6.67.

**Author Contributions:** Conceptualisation, J.Z. and Z.M.; methodology, J.Z. and Z.M.; software, X.C. and J.Z.; validation, J.Z. and X.C.; formal analysis, J.Z. and X.C.; investigation, J.Z. and X.C.; resources, Y.W.; data curation, X.C., J.Z. and Z.M.; writing—original draft preparation, J.Z.; writing—review and editing, Z.M. and J.Z.; visualisation, X.C. and J.Z.; supervision, D.C., Z.M., Y.W. and A.P.R.; project administration, Z.M. and J.Z.; funding acquisition, Z.M. and J.Z. All authors have read and agreed to the published version of the manuscript.

**Funding:** This research was funded by Engineering and Physical Sciences Research Council, grant number EP/V042564/1.

**Data Availability Statement:** Not applicable.

**Acknowledgments:** I would like to express my deep gratitude to Ke Tang, for her patient guidance, enthusiastic encouragement, and useful critiques of this research work. I would also like to thank Pan Wang, for her advice and assistance in keeping my progress on schedule. I would also like to extend my thanks to the technicians of the laboratory for their help in offering me the resources in running the program.

**Conflicts of Interest:** The authors declare no conflict of interest. The funders had no role in the design of the study; in the collection, analyses, or interpretation of data; in the writing of the manuscript; or in the decision to publish the results.

## References

1. Kuravi, S.; Trahan, J.; Goswami, Y.D.; Rahman, M.M.; Stefanakos, E.K. Thermal energy storage technologies and systems for concentrating solar power plants. *Prog. Energy Combust. Sci.* **2013**, *39*, 285–319. [[CrossRef](#)]
2. Mahlia, T.M.I.; Saktisahdan, T.J.; Jannifar, A.; Hasan, M.H.; Matseelar, H.S.C. A review of available methods and development on energy storage; technology update. *Renew. Sustain. Energy Rev.* **2014**, *33*, 532–545. [[CrossRef](#)]
3. Pardo, P.; Deydier, A.; Anxionnaz-Minvielle, Z.; Rougé, S.; Cabassud, M.; Cognet, P. A review on high temperature thermochemical heat energy storage. *Renew. Sustain. Energy Rev.* **2014**, *32*, 591–610. [[CrossRef](#)]
4. Yan, T.; Wang, R.Z.; Li, T.X.; Wang, L.W.; Fred, I.T. A review of promising candidate reactions for chemical heat storage. *Renew. Sustain. Energy Rev.* **2015**, *43*, 13–31. [[CrossRef](#)]
5. Li, T.X.; Wu, S.; Yan, T.; Wang, R.Z.; Zhu, J. Experimental investigation on a dual-mode thermochemical sorption energy storage system. *Energy* **2017**, *140*, 383–394. [[CrossRef](#)]
6. Whiting, G.; Grondin, D.; Bennici, S.; Auroux, A. Heats of water sorption studies on zeolite-MgSO<sub>4</sub> composites as potential thermochemical heat storage materials. *Sol. Energy Mater. Sol. Cells* **2013**, *112*, 112–119. [[CrossRef](#)]

7. Liu, M.; Tay, N.H.S.; Bell, S.; Belusko, M.; Jacob, R.; Will, G.; Saman, W.; Bruno, F. Review on concentrating solar power plants and new developments in high temperature thermal energy storage technologies. *Renew. Sustain. Energy Rev.* **2016**, *53*, 1411–1432. [[CrossRef](#)]
8. Mazzoni, S.; Ooi, S.; Nastasi, B.; Romagnoli, A. Energy storage technologies as techno-economic parameters for master-planning and optimal dispatch in smart multi energy systems. *Appl. Energy* **2019**, *254*, 113682. [[CrossRef](#)]
9. Ryu, J.-Y.; Alford, A.; Lewis, G.; Ding, Y.; Li, Y.; Ahmad, A.; Kim, H.; Park, S.-H.; Park, J.-P.; Branch, S.; et al. A novel liquid air energy storage system using a combination of sensible and latent heat storage. *Appl. Therm. Eng.* **2021**, *203*, 117890. [[CrossRef](#)]
10. Bellan, S.; Gonzalez-Aguilar, J.; Romero, M.; Rahman, M.M.; Goswami, D.Y.; Stefanakos, E.K.; Couling, D. Numerical analysis of charging and discharging performance of a thermal energy storage system with encapsulated phase change material. *Appl. Therm. Eng. Des. Process. Equip. Econ.* **2014**, *71*, 481–500. [[CrossRef](#)]
11. Abedin, A.H.; Rosen, M.A. A critical review of thermochemical energy storage systems. *Open Renew. Energy J.* **2011**, *4*, 42–46. [[CrossRef](#)]
12. Aydin, D.; Casey, S.P.; Riffat, S. The latest advancements on thermochemical heat storage systems. *Renew. Sustain. Energy Rev.* **2015**, *41*, 356–367. [[CrossRef](#)]
13. Schmidt, M.; Szczukowski, C.; Roßkopf, C.; Linder, M.; Wörner, A. Experimental results of a 10 kW high temperature thermochemical storage reactor based on calcium hydroxide. *Appl. Therm. Eng.* **2014**, *62*, 553–559. [[CrossRef](#)]
14. Li, W.; Luo, X.; Yang, P.; Wang, Q.; Zeng, M.; Markides, C.N. Solar-thermal energy conversion prediction of building envelope using thermochemical sorbent based on established reaction kinetics. *Energy Convers. Manag.* **2021**, *252*, 115117. [[CrossRef](#)]
15. Scapino, L.; Zondag, H.A.; Van Bael, J.; Diriken, J.; Rindt, C.C.M. Sorption heat storage for long-term low-temperature applications: A review on the advancements at material and prototype scale. *Appl. Energy* **2017**, *190*, 920–948. [[CrossRef](#)]
16. Lizana, J.; Chacartegui, R.; Barrios-Padura, A.; Valverde, J.M. Advances in thermal energy storage materials and their applications towards zero energy buildings: A critical review. *Appl. Energy* **2017**, *203*, 219–239. [[CrossRef](#)]
17. Cabeza, L.F.; Solé, A.; Barreneche, C. Review on sorption materials and technologies for heat pumps and thermal energy storage. *Renew. Energy* **2017**, *110*, 3–39. [[CrossRef](#)]
18. Gaeini, M.; Zondag, H.; Rindt, C. Effect of kinetics on the thermal performance of a sorption heat storage reactor. *Appl. Therm. Eng.* **2016**, *102*, 520–531. [[CrossRef](#)]
19. Donkers, P.A.J.; Sogutoglu, L.C.; Huinink, H.P.; Fischer, H.R.; Adan, O.C.G. A review of salt hydrates for seasonal heat storage in domestic applications. *Appl. Energy* **2017**, *199*, 45–68. [[CrossRef](#)]
20. Bertsch, F.; Mette, B.; Asenbeck, S.; Kerskes, H.; Müller-Steinhagen, H. Low temperature chemical heat storage—An investigation of hydration reactions. In Proceedings of the 11th Int. Conference on Thermal Energy Storages (Effstock), Stockholm, Sweden, 14–17 June 2009.
21. Molenda, M.; Bouché, M.; Linder, M.; Blug, M.; Busse, J.; Wörner, A. Thermochemical energy storage for low temperature applications: Materials and first studies in a gas-solid reactor. In Proceedings of the 12th Int. Conference on Energy Storage (Innostock), Lleida, Spain, 16–18 May 2012.
22. Zondag, H.; Kikkert, B.; Smeding, S.; de Boer, R.; Bakker, M. Prototype thermochemical heat storage with open reactor system. *Appl. Energy* **2013**, *109*, 360–365. [[CrossRef](#)]
23. Yu, N.; Wang, R.Z.; Lu, Z.S.; Wang, L.W. Development and characterisation of silica gel-LiCl composite sorbents for thermal energy storage. *Chem. Eng. Sci.* **2014**, *111*, 73–84. [[CrossRef](#)]
24. Yu, N.; Wang, R.Z.; Lu, Z.S.; Wang, L.W. Study on consolidated composite sorbents impregnated with LiCl for thermal energy storage. *Int. J. Heat Mass Trans.* **2015**, *84*, 660–670. [[CrossRef](#)]
25. Brancato, V.; Calabrese, L.; Palomba, V.; Frazzica, A.; Fullana-Puig, M.; Solé, A.; Cabeza, L.F. MgSO<sub>4</sub>·7H<sub>2</sub>O filled macro cellular foams: An innovative composite sorbent for thermo-chemical energy storage applications for solar buildings. *Sol. Energy* **2018**, *173*, 1278–1286. [[CrossRef](#)]
26. Piperopoulos, E.; Calabrese, L.; Bruzzaniti, P.; Brancato, V.; Palomba, V.; Caprì, A.; Frazzica, A.; Cabeza, L.F.; Proverbio, E.; Milone, C. Morphological and Structural Evaluation of Hydration/Dehydration Stages of MgSO<sub>4</sub> Filled Composite Silicone Foam for Thermal Energy Storage Applications. *Appl. Sci.* **2020**, *10*, 453. [[CrossRef](#)]
27. Zhao, H.Z.; Wang, Z.Y.; Li, Q.W.; Wu, T.H.; Zhang, M.; Shi, Q.Q. Water sorption on composite material “zeolite 13X modified by LiCl and CaCl<sub>2</sub>”. *Microporous Mesoporous Mater.* **2020**, *299*, 110109. [[CrossRef](#)]
28. Macriss, R.A.; Gutraj, J.; Zawacki, T.S. *Absorption Fluid Data Survey: Final Report on Worldwide Data*; Oak Ridge National Lab.: Oak Ridge, TN, USA; Institute of Gas Technology: Chicago, IL, USA, 1988.
29. Posern, K.; Kaps, C. Calorimetric studies of thermochemical heat storage materials based on mixtures of MgSO<sub>4</sub> and MgCl<sub>2</sub>. *Thermochim. Acta* **2010**, *502*, 73–76. [[CrossRef](#)]
30. Gordeeva, L.G.; Grekova, A.D.; Krieger, T.A.; Aristov, Y.I. Adsorption properties of composite materials (LiCl+LiBr)/silica. *Microporous Mesoporous Mater.* **2009**, *126*, 262–267. [[CrossRef](#)]
31. Entezari, A.; Ge, T.S.; Wang, R.Z. Water adsorption on the coated aluminum sheets by composite materials (LiCl + LiBr)/silica gel. *Energy* **2018**, *160*, 64–71. [[CrossRef](#)]
32. Druske, M.; Fopah-lele, A.; Korhammer, K.; Urs, H. Developed materials for thermal energy storage: Synthesis and characterization. *Energy Procedia* **2014**, *61*, 96–99. [[CrossRef](#)]
33. Mohapatra, D.; Nandanavanam, J. Salt in matrix for thermochemical energy storage—A review. *Mater. Today Proc.* **2022**. [[CrossRef](#)]

34. Lim, K.; Che, J.; Lee, J. Experimental study on adsorption characteristics of a water and silica-gel based thermal energy storage (TES) system. *Appl. Therm. Eng.* **2017**, *110*, 80–88. [[CrossRef](#)]
35. Erlund, R.; Zevenhoven, R. Thermal energy storage (TES) capacity of a lab scale magnesium hydro carbonates/silica gel system. *J. Energy Storage* **2019**, *25*, 100907. [[CrossRef](#)]
36. Mahon, D.; Claudio, G.; Eames, P. A study of novel high performance and energy dense zeolite composite materials for domestic interseasonal thermochemical energy storage. *Energy Procedia* **2019**, *158*, 4489–4494. [[CrossRef](#)]
37. Whiting, G.; Grondin, D.; Bennici, S.; Auroux, A.; Boer, D.R.; Smeding, S.F.; Zondag, H.A.; Krol, G. *Development of a Prototype System for Seasonal Solar Heat Storage Using an Open Sorption Process*; ECN: Petten, The Netherlands, 2014; Volume 99, pp. 1–9.
38. Singh, A.P.; Khanna, S.; Paneliya, S.; Hinsu, H.; Patel, Y.; Mehta, B. Preparation and characterisation of solid-state neopentyl glycol/expanded graphite micro composite for thermal energy storage applications. *Mater. Today Proc.* **2021**, *47*, 621–625. [[CrossRef](#)]
39. Xu, C.; Yu, Z.B.; Xie, Y.Y.; Ren, Y.X.; Ye, F.; Ju, X. Study of the hydration behavior of zeolite-MgSO<sub>4</sub> composites for long-term heat storage. *Appl. Therm. Eng.* **2018**, *129*, 250–259. [[CrossRef](#)]
40. Nonnen, T.; Preißler, H.; Kött, S.; Beckert, S.; Gläser, R. Salt inclusion and deliquescence in salt/zeolite X composites for thermochemical heat storage. *Microporous Mesoporous Mater.* **2020**, *303*, 110239. [[CrossRef](#)]
41. Zhang, Y.N.; Wang, R.Z.; Zhao, Y.J.; Li, T.X.; Riffat, S.B.; Wajid, N.M. Development and thermochemical characterisations of vermiculite/SrBr<sub>2</sub> composite sorbents for low-temperature heat storage. *Energy* **2016**, *115*, 120–128. [[CrossRef](#)]
42. Wang, Q.; Xie, Y.Y.; Ding, B.; Yu, G.L.; Ye, F.; Xu, C. Structure and hydration state characterisations of MgSO<sub>4</sub>-zeolite 13x composite materials for long-term thermochemical heat storage. *Sol. Energy Mater. Sol. Cells* **2019**, *200*, 110047. [[CrossRef](#)]
43. Wei, S.; Zhou, W.; Han, R.; Gao, J.; Zhao, G.; Qin, Y.; Wang, C. Influence of minerals with different porous structures on thermochemical heat storage performance of CaCl<sub>2</sub>-based composite sorbents. *Sol. Energy Mater. Sol. Cells* **2022**, *243*, 111769. [[CrossRef](#)]
44. Ge, Y.Q.; Zhao, Y.; Zhao, C.Y. Transient simulation and thermodynamic analysis of pumped thermal electricity storage based on packed-bed latent heat/cold stores. *Renew. Energy* **2021**, *174*, 939–951. [[CrossRef](#)]
45. Calabrese, L.; Antonellis, D.S.; Vasta, S.; Brancato, V.; Freni, A. Modified Silicone-SAPO34 Composite Materials for Adsorption Thermal Energy Storage Systems. *Appl. Sci.* **2020**, *10*, 8715. [[CrossRef](#)]
46. Xu, C.; Xie, Y.Y.; Liao, Z.R.; Ren, Y.; Ye, F. Numerical study on the desorption process of a thermochemical reactor filled with MgCl<sub>2</sub>·6H<sub>2</sub>O for seasonal heat storage. *Appl. Therm. Eng.* **2019**, *146*, 785–794. [[CrossRef](#)]
47. Li, W.; Klemeš, J.J.; Wang, Q.W.; Zeng, M. Development and characteristics analysis of salt-hydrate based composite sorbent for low-grade thermochemical energy storage. *Renew. Energy* **2020**, *157*, 920–940. [[CrossRef](#)]
48. Safa, A.A.; Fung, A.S.; Kumar, R. Heating and cooling performance characterisation of ground source heat pump system by testing and TRNSYS simulation. *Renew. Energy* **2015**, *83*, 565–575. [[CrossRef](#)]
49. Sakellari, D.; Forsén, M.; Lundqvist, P. Investigating control strategies for a domestic low-temperature heat pump heating system. *Int. J. Refrig.* **2006**, *29*, 547–555. [[CrossRef](#)]
50. Voottipruex, K.; Sangswang, A.; Naetiladdanon, S.; Mujjalinvimut, E.; Wongyao, N. PEM fuel cell emulator based on dynamic model with relative humidity calculation. In Proceedings of the 2017 14th International Conference on Electrical Engineering/Electronics, Computer, Telecommunications and Information Technology (ECTI-CON), Phuket, Thailand, 27–30 June 2017; pp. 529–532.
51. Zhao, Y.J.; Wang, R.Z.; Zhang, Y.N.; Yu, N. Development of SrBr<sub>2</sub> composite sorbents for a sorption thermal energy storage system to store low-temperature heat. *Energy* **2016**, *115*, 129–139. [[CrossRef](#)]
52. Zhang, Y.N.; Wang, R.Z.; Li, T.X. Experimental investigation on an open sorption thermal storage system for space heating. *Energy* **2017**, *141*, 2421–2433. [[CrossRef](#)]
53. Jarre, M.; Noussan, M.; Simonetti, M. Primary energy consumption of heat pumps in high renewable share electricity mixes. *Energy Convers. Manag.* **2018**, *171*, 1339–1351. [[CrossRef](#)]
54. Martinek, J.; Jorgenson, J.; McTigue, J.D. On the operational characteristics and economic value of pumped thermal energy storage. *J. Energy Storage* **2022**, *52*, 105005. [[CrossRef](#)]